Partial rescue of the prophase I defects of *Atm*-deficient mice by *p53* and *p21* null alleles

Carrolee Barlow[1*], Marek Liyanage[2*], Peter B. Moens[3], Chu-Xia Deng[4], Thomas Ried[2] & Anthony Wynshaw-Boris[1]

Patients with the human disorder ataxia-telangiectasia (A-T; refs 1,2) and *Atm*-deficient mice[3–5] have a pleiotropic phenotype that includes infertility. Here we demonstrate that male gametogenesis is severely disrupted in *Atm*-deficient mice in the earliest stages of meiotic prophase I, resulting in apoptotic degeneration. Atm is required for proper assembly of Rad51 onto the chromosomal axial elements during meiosis. In addition, p53, p21 and Bax are elevated in testes from *Atm*-deficient mice. To determine whether these elevated protein levels are important factors in the meiotic disruption of *Atm*-deficient mice, we analysed the meiotic phenotype of *Atm/p53* or *Atm/p21* double mutants. In these double mutants, meiosis progressed to later stages but was only partly rescued. Assembly of Rad51 foci on axial elements remained defective, and gametogenesis proceeded only to pachytene of prophase I. Previous results demonstrated that mice homozygous for a null mutation in *Rad51* (ref. 6) display an early embryonic lethal phenotype that can be partly rescued by removing p53 and/or p21. Because *Atm*-deficient mice are viable but completely infertile, our studies suggest that the Rad51 assembly defects and elevated levels of p53, p21 and Bax represent tissue-specific responses to the absence of Atm.

Mammalian Rad51 is localized to the unpaired axial elements and paired synaptonemal complexes during prophase I of meiosis in association with the axial element protein Cor1 (ref. 7). Bright Rad51 foci (green) were associated exclusively with Cor1 (yellow) on the forming axial cores in leptotene and zygotene spermatocytes from wild-type mice (arrows in Fig. 1*a*,*b*). Early in pachytene (arrow in Fig. 1*c*), only a few Rad51 foci remained along the synaptonemal complexes. Similarly, Cor1 was localized to the axial elements of early prophase spermatocytes from *Atm*-deficient mice (Fig. 1*d* arrows). In contrast to the wild-type pattern, however, no bright Rad51 foci were detected in these spermatocytes (Fig. 1*e*). Occasionally, weaker Cor1-associated Rad51 signals were present (arrows in Fig. 1*e–f*), but a substantial fraction of weaker Rad51 signals were mislocalized to chromatin (arrowheads in Fig. 1*e–f*), a pattern not seen in spermatocytes from wild-type mice. Thus, *Atm* deficiency is associated with a failure of proper Rad51 assembly onto the axial elements.

p53 is induced by Atm in the thymus in response to ionizing radiation[8], and p21 (ref. 9) and Bax (ref. 10) are, in turn, induced by p53. p53 and p21 were present at undetectable levels in testes from wild-type mice, but p53 and p21 basal levels were much higher in testes from *Atm*-deficient mice (Fig. 2). Basal levels of Bax were clearly detectable in testes of wild-type mice, and, like p53 and p21, Bax was present at higher baseline levels in *Atm*-deficient than in wild-type testes. Such elevations are not observed in other tissues from *Atm*-deficient mice (data not shown), suggesting that meiotic cells specifically display this response to *Atm* deficiency. These results indicate that high levels of p53, p21 and Bax proteins contribute to the severe meiotic phenotype of *Atm*-deficient mice.

To test this hypothesis, we generated liveborn male mice with the following genotypes: $Atm^{-/-}p53^{+/-}$, $Atm^{-/-}p53^{-/-}$ and $Atm^{-/-}p21^{-/-}$. *p53* (ref. 11) and *p21* (ref. 12) mutant mice have normal fertility. Testes from each of these double mutants were larger than testes from $Atm^{-/-}$ mice, although not as big as those of wild-type mice (data not shown). Histologically, spermatogenesis was improved in double mutants, compared with *Atm*-deficient mice (Fig. 3). All stages of spermatogenesis were observed in sections from control mice (Fig. 3*a*,*f*), and as previously reported[3], most seminiferous tubules from *Atm*-deficient mice consisted of spermatogonia, degenerating spermatocytes and Sertoli cells (Fig. 3*b*,*g*). In contrast, numerous cells with the appearance of pachytene spermatocytes (arrowheads) were observed in tubules from $Atm^{-/-}p53^{+/-}$ (Fig. 3*c*,*h*), $Atm^{-/-}p53^{-/-}$ (Fig. 3*d*,*i*) and $Atm^{-/-}p21^{-/-}$ (Fig. 3*e*,*j*) mice. However, no mature sperm were observed in tubules from any of the three double-mutant genotypes, and animals were infertile (data not shown).

Improvement of spermatocyte morphology in double-mutant mice was associated with, but not proportional to, decreases in apoptosis as measured by the TUNEL *in situ* assay. In tubules from control mice (Fig. 3*k*) there were few apoptotic cells, whereas tubules from *Atm*-deficient mice (Fig. 3*l*) had numerous apoptotic cells. Apoptosis was reduced by 27% in tubules from $Atm^{-/-}p53^{+/-}$ mice (Fig. 3*m*), by 70% in tubules from $Atm^{-/-}p53^{-/-}$ mice (Fig. 3*n*) and by 40% in tubules from $Atm^{-/-}p21^{-/-}$ mice (Fig. 3*o*), compared with tubules from *Atm*-deficient mice (Fig. 3*l*). Improvement in spermatocyte morphology was not proportional to changes in apoptosis. In particular, apoptosis was similar for $Atm^{-/-}p21^{-/-}$ and $Atm^{-/-}p53^{+/-}$ tubules, yet histological improvement was greater in $Atm^{-/-}p21^{-/-}$ than $Atm^{-/-}p53^{+/-}$ tubules. In addition, morphological improvement was similar for $Atm^{-/-}p21^{-/-}$ and $Atm^{-/-}p53^{-/-}$ tubules, but there were substantial differences in levels of apoptosis.

Synaptonemal complex morphology was examined with a mixture of antibodies to centromeric proteins Cor1 and Syn1 to stain axial elements. In surface spreads of spermatocytes from wild-type mice (Fig. 3*p*), mature pachytene synaptonemal complexes were routinely observed; in spreads from *Atm*-deficient mice (Fig. 3*q*), fragmented complexes were seen and no pachytene-type complexes were detected. In contrast, nearly normal pachytene complexes were observed in spreads from $Atm^{-/-}p53^{+/-}$ (Fig. 3*r*), $Atm^{-/-}p53^{-/-}$ (Fig. 3*s*) and $Atm^{-/-}p21^{-/-}$ (Fig. 3*t*) spermatocytes. In support of this, we used histone H1t, a testes-specific H1 histone that associates with chromatin of meiotic spermatocytes in middle to late pachytene[13], as a marker. We saw no H1t staining of spermatocyte spreads from *Atm*-deficient-mice, as expected, but

[1]*Laboratory of Genetic Disease Research,* [2]*Genome Technology Branch, National Human Genome Research Institute;* [4]*Laboratory of Biochemistry and Metabolism, National Institute of Diabetes, Digestive and Kidney Disorders, National Institutes of Health, Bethesda, Maryland 20892, USA.* [3]*Department of Biology, York University, Downsview, Ontario M3J 1P3, Canada.* *C.B. and M.L. contributed equally to this work. Correspondence should be addressed to A.W.-B. e-mail: tonywb@nhgri.nih.gov*

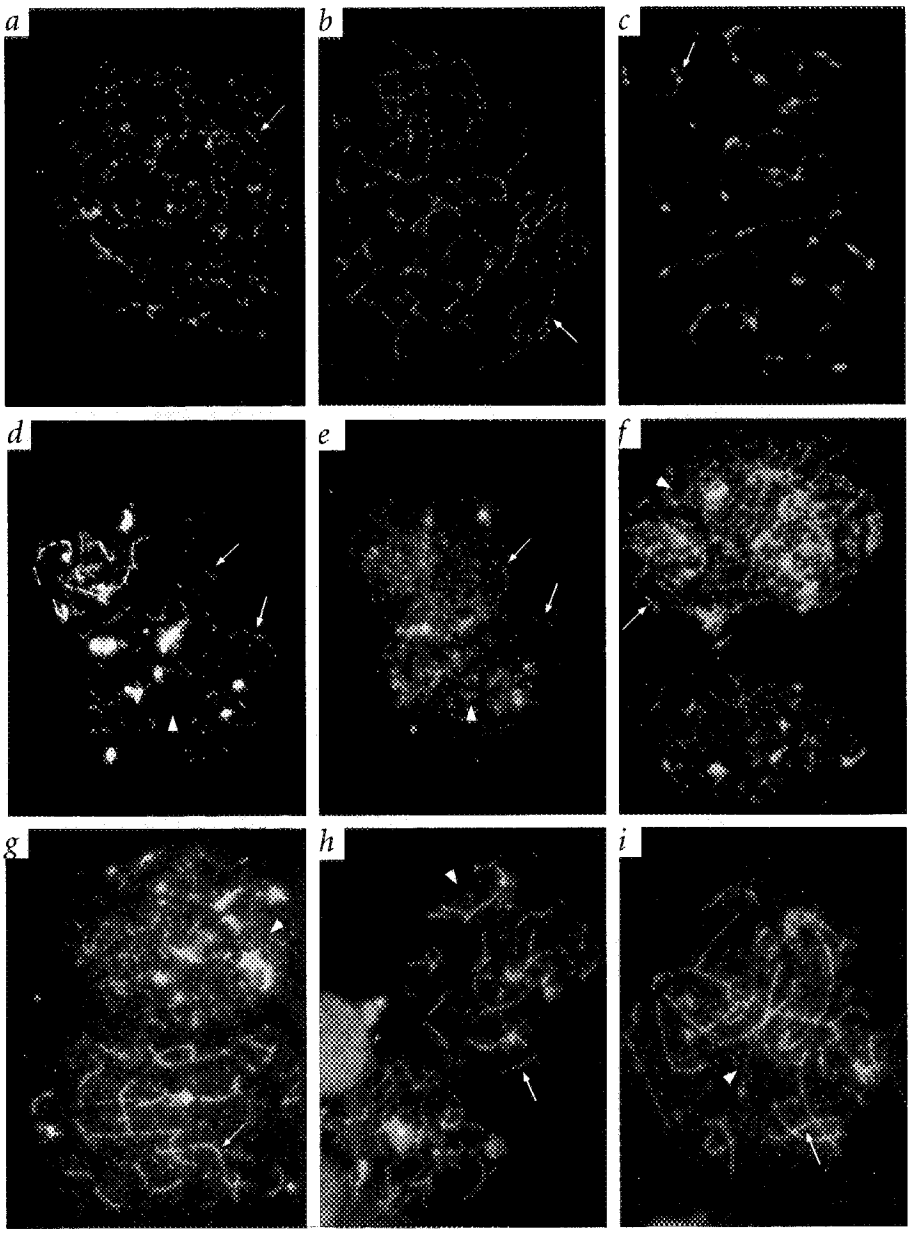

Fig. 1 Rad51 localization in leptotene-zygotene spermatocytes. Surface spreads from the following genotypes were used: wild-type (***a***, leptotene; ***b***, zygotene; ***c***, pachytene), $Atm^{-/-}$ (***d–f***), $Atm^{-/-}p53^{+/-}$ (***g***); $Atm^{-/-}p53^{-/-}$ (***h***) and $Atm^{-/-}p21^{-/-}$ (***i***). Synaptonemal complexes were stained simultaneously with antibodies to Rad51 (green) and Cor1 (yellow); photomicrographs of Cor1 staining (***d***), Rad51 staining (***e***) or Rad51 and Cor1 staining overlaid (***a–c***, ***f–i***) are shown. Exposure times for Rad51 were 30 s in *a–c* and 2 min in *d–i*. Arrows in all panels indicate examples of Rad51 foci co-localizing with Cor1; arrowheads represent areas where Rad51 foci are on chromatin, not associated with Cor1.

detected H1t-positive cells in spreads from double mutant animals (data not shown). These pachytene synaptonemal complexes were not entirely normal, as complexes or fragments of complexes without centromeres (arrows in Fig. 3*r–s*) and complexes with two centromeres (yellow arrow in Fig. 3*s*) were present. In addition, not all cells in spreads from double-mutant mice had pachytene morphology.

Electron-microscopic analysis demonstrated that synaptonemal complex morphology of spreads from $Atm^{-/-}p53^{+/-}$ (Fig. 4*c*), $Atm^{-/-}p53^{-/-}$ (Fig. 4*d*) and $Atm^{-/-}p21^{-/-}$ (Fig. 4*e*) mice was improved compared with spreads from $Atm^{-/-}$ mice (Fig. 4*b*), but not entirely normal. In comparison with spreads from wild-type mice (Fig. 4*a*), synaptonemal complex length was more variable and shorter, and more than twenty fragments of complexes were observed in all double mutants (data not shown). Axial gaps were often observed in spreads from *Atm*-deficient mice (Fig. 4*f*), but not in the spermatocyte spreads from the double mutants (Fig. 4*g*). Consistent with results described above, diplotene stages with chiasma formation were not detected in double-mutant spermatocyte spreads. Thus, p53 or p21 deficiency allowed progression to pachytene stages of meiosis I in *Atm*-deficient mice, but diplotene was not achieved in double-mutant mice.

Surprisingly, p21 and Bax or p53 and Bax basal levels were substantially elevated in testes from *Atm/p53* or *Atm/p21* double-mutant mice, respectively, to levels as high as in $Atm^{-/-}$ mice (Fig. 2). However, these elevated protein levels were a consequence of loss of *Atm* function, as p21 and Bax were not elevated in testes from $Atm^{+/+}p53^{-/-}$ or $Atm^{+/+}p53^{+/-}$ mice, and p53 and Bax were not elevated in $Atm^{+/+}p21^{-/-}$ mice (Fig. 2). In addition, as in spreads from *Atm*-deficient mice (Fig. 1*f*), bright Rad51 foci were not detected on the axial elements in spreads from

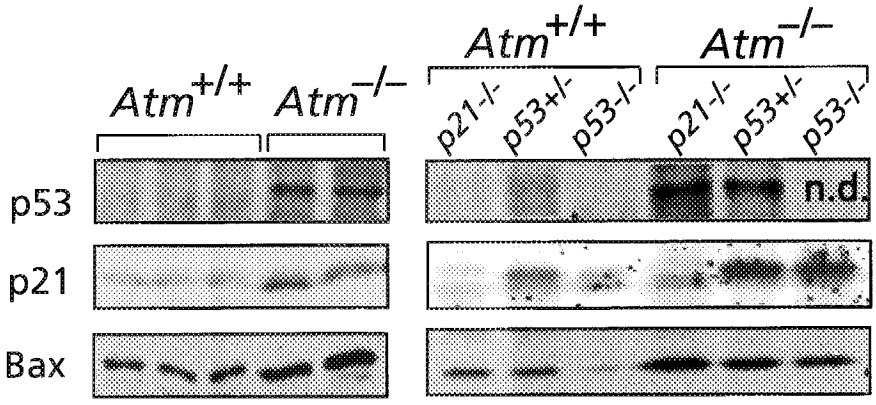

Fig. 2 p53, p21 and Bax expression in testes. Expression levels in testes from wild-type and $Atm^{-/-}$ mice, $p53^{+/-}$, $p53^{-/-}$ and $p21^{-/-}$ single mutants or *Atm/p53* and *Atm/p21* double mutants are shown. Boxes surround immunoblots from individual gels, although lanes were shifted in the p53 blot on the right for consistency in labelling. n.d., not done.

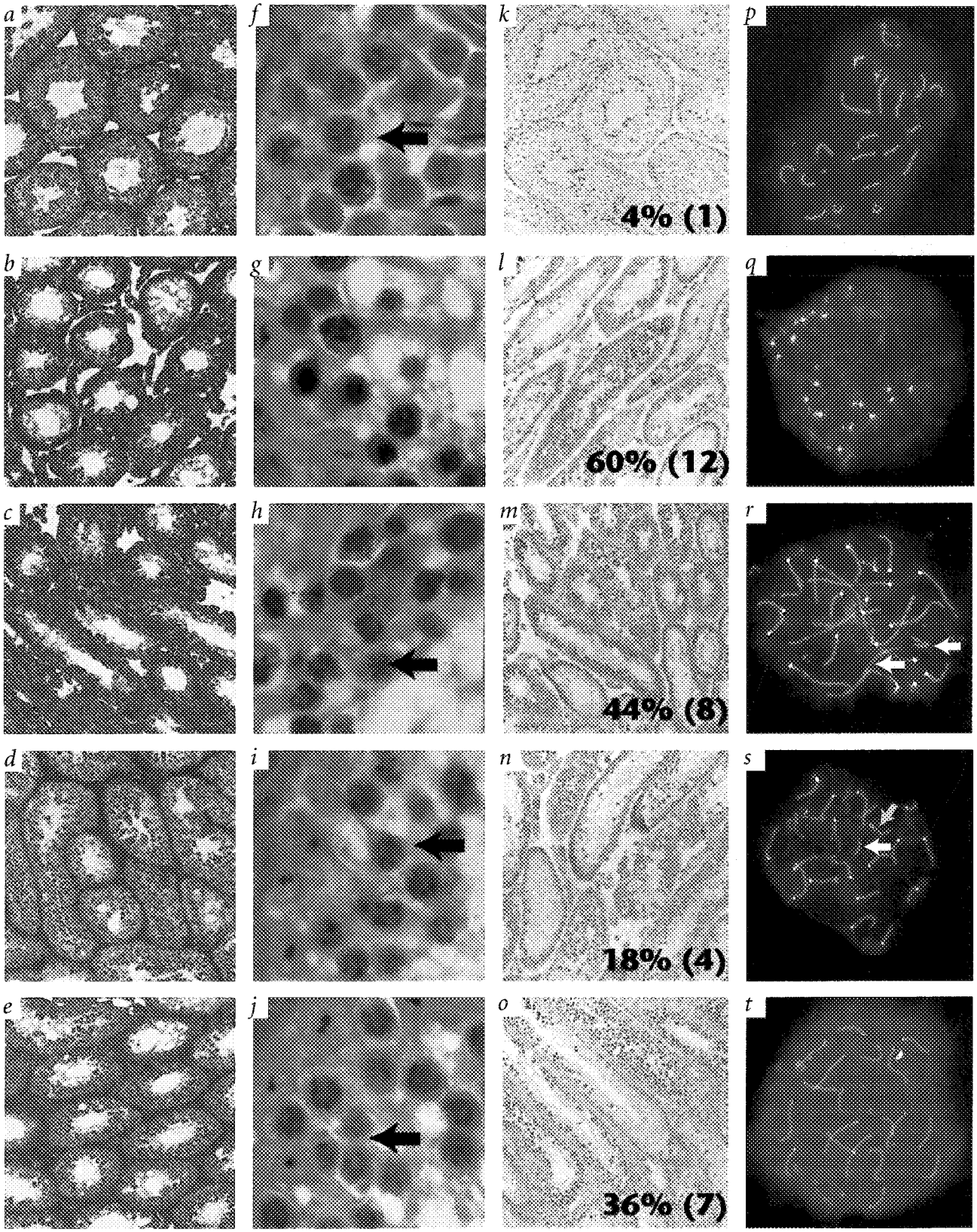

Fig. 3 Seminiferous tubule morphology, apoptosis and fluorescent synaptonemal complex immunostaining of surface spreads of pachytene spermatocytes from wild-type and single- or double-mutant mice. The following genotypes were examined: control *Atm*$^{+/-}$*p53*$^{-/-}$ (***a***,***f***,***k***,***p***), *Atm*$^{-/-}$ (***b***,***g***,***l***,***q***), *Atm*$^{-/-}$*p53*$^{+/-}$ (***c***,***h***,***m***,***r***), *Atm*$^{-/-}$*p53*$^{-/-}$ (***d***,***i***,***n***,***s***) and *Atm*$^{-/-}$*p21*$^{-/-}$ (***e***,***j***,***o***,***t***). Single seminiferous tubules were embedded in plastic, sectioned and stained with toluidine blue at ×20 (***a***–***e***) and ×100 (***f***–***j***) magnification. Apoptosis was examined at ×20 with the TUNEL *in situ* assay (***k***–***o***). Fifty randomly selected tubules of each genotype were examined. The percentage of tubules with any apoptotic cells is displayed at the bottom of each panel, with the average number of apoptotic cells in positive tubules shown in parentheses. Pachytene spermatocytes were stained with an anti-centromere antibody (white) and a mixture of Cor1 and Syn1 (yellow) for examination of synaptonemal complexes (***p***–***t***). Arrows, complexes or fragments without centromeres; yellow arrow, a complex with two centromeres. *Atm*$^{+/-}$*p53*$^{-/-}$ mice were used as controls, to allow direct comparison with *Atm/p53* double-mutant mice, but identical results were observed with wild-type mice (data not shown).

Atm$^{-/-}$*p53*$^{+/-}$ (Fig. 1*g*), *Atm*$^{-/-}$*p53*$^{-/-}$ (Fig. 1*h*) and *Atm*$^{-/-}$*p21*$^{-/-}$ (Fig. 1*i*) spermatocytes. Weaker Rad51 foci were present on axial elements (arrows) and associated with chromatin (arrowheads) in all three double-mutant genotypes.

The Rad51 assembly defects were not rescued in double mutants, nor were the elevated levels of p53, p21 and Bax, suggesting that in the testes, p53 pathways are downstream of Rad51, or that p53 and Rad51 pathways are independently affected by the absence of Atm. In addition, it appears that without appropriate localization of Rad51, meiosis cannot proceed beyond pachytene. We do not know whether Rad51 assembly is directly or indirectly regulated by Atm, as we have not observed co-localization of Rad51 and Atm on meiotic chromosomes (data not shown). Atm may be required for the assembly of Rad51 on axial elements in preparation for meiotic recombination. Alternatively, Atm may provide a meiotic checkpoint function necessary for monitoring a process before Rad51 assembly, to ensure that the process is complete before Rad51 assembly is attempted. This dysregulation of meiosis appears to result in higher levels of p53 and downstream genes, perhaps because of the activation of surveillance functions of p53 (refs 18,19). We do not know, however, whether Rad51 assembly defects are directly responsible for these elevated levels.

Our results demonstrate an association between Atm and Rad51 function, which may provide insight into other phenotypes seen in AT patients and heterozygous carriers. Recent studies have demonstrated that proteins encoded by the familial breast-cancer susceptibility genes *BRCA1* and *BRCA2* physically interact with Rad51 (refs 14,15). Mice homozygous for null mutations of *Brca1*(refs 16,17), *Brca2* (ref. 17) or *Rad51* (ref. 6) display similar early embryonic lethal phenotypes that are partly rescued by removal of *p53* and/or *p21*. Similarly, Atm participates in the regulation of Rad51 assembly during meiosis, and the meiotic phenotype is partly rescued by *p53* or *p21* deficiency. This severe phenotype associated with Rad51 and p53 dysregulation appears to be exclusive to meiotic cells. However, if Atm were important for Rad51 function in somatic cells, it might participate with Brca1 and Brca2 in the regulation of Rad51 activity. Perturbation of these interactions or regulation might then result in a higher frequency of malignancy in AT patients, as well as carriers of mutations in *AT, BRCA1* and *BRCA2*.

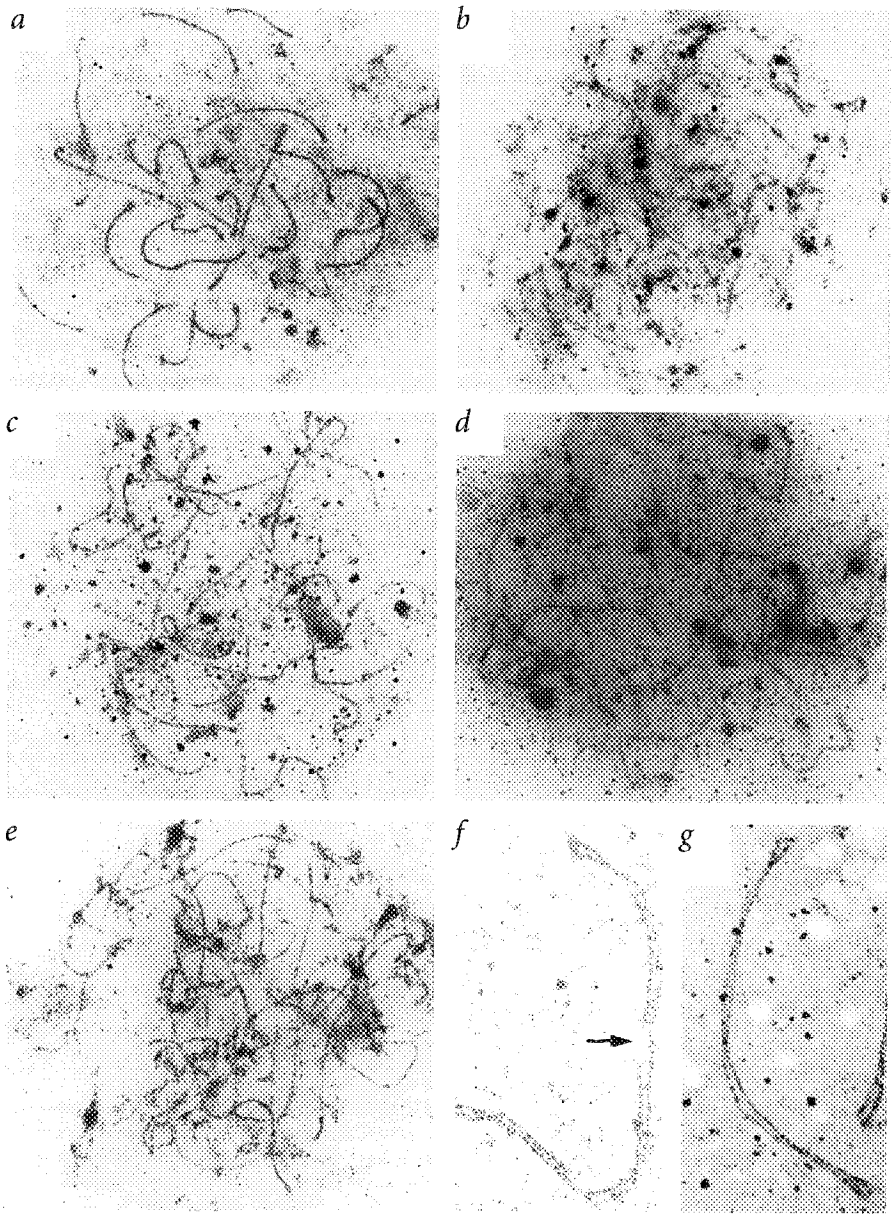

Fig. 4 Examination of synaptonemal complexes by transmission electron microscopy. Shown are silver-stained preparations of microspreads of spermatocytes from *Atm*$^{+/-}$*p53*$^{-/-}$ (**a**), *Atm*$^{-/-}$*p53*$^{+/+}$ (**b**), *Atm*$^{-/-}$*p53*$^{+/-}$ (**c**), *Atm*$^{-/-}$*p53*$^{-/-}$ (**d**) and *Atm*$^{-/-}$*p21*$^{-/-}$ (**e**) mice. Higher-magnification views of synaptonemal complexes from *Atm*-deficient spermatocytes (**f**) and *Atm*$^{-/-}$*p21*$^{-/-}$ spermatocytes (**g**) are shown. Note the axial gap in the complex from the *Atm*$^{-/-}$ spermatocyte (*f*, arrow). *Atm*$^{+/-}$*p53*$^{-/-}$ mice were used as controls, to allow direct comparison with *Atm/p53* double-mutant mice, but identical results were observed with wild-type mice (data not shown).

Methods

Mating and genotyping mice. The creation of the *Atm*-deficient mice (allele designation $Atm^{ins5790neo}$) was previously described[3]. Mice from heterozygous crosses were genotyped by Southern blotting as described[3], using *Eco*RV-digested DNA and a genomic probe surrounding the targetted exon. Heterozygotes were derived from mating in a completely inbred 129SvEv background.

p53-deficient mice[11] were obtained from Jackson Laboratories and genotyped by PCR. *p21*-deficient mice were created and genotyped by PCR as described[12]. To create mice deficient for *Atm* and *p53*, offspring from double heterozygous crosses were genotyped for both genes as described above. To create mice deficient for both *Atm* and *p21*, $Atm^{+/-}p21^{-/-}$ mice were crossed and offspring genotyped as described[12].

Histological analysis. Testes and ovaries were isolated and fixed in 20 V 10% buffered formalin. Fixed tissues were embedded in paraffin or plastic, sectioned and stained according to standard methods[20] by American HistoLabs. Sections were examined and photographed under light microscopy. For TUNEL assays, paraffin-embedded sections were dewaxed and analysed with the TACS *in situ* kit (Trevigen).

Preparation of male meiotic prophase spermatocytes. Meiotic prophases were prepared by the surface microspreading technique[21] to allow sequential analysis of microspreads by light and transmission electron microscopy. In brief, a single cell suspension was prepared from testes of two-month-old male mice. Cells were lysed in hypotonic salt (0.50 mM, pH 8.0), and nuclei attached to glass or plastic-coated microscope slides. Nuclei were fixed for 6 min (2% paraformaldehyde, with or without 0.03% SDS, pH 8.2). After several washes with Photoflo (0.4% Kodak Photoflo 600 in distilled water, pH 8.2), slides were dried; they were stained for approximately 90 min at 60 °C with a silver staining solution (50% silver nitrate, 0.03% formalin in distilled water). After de-staining in distilled water, slides were air-dried. Photographic images at the light microscopy level were acquired with a ×100 objective.

For electron microscopy, slides were immersed in 30–50% silver nitrate, covered with nylon mesh and incubated in a moist environment for 10–30 min. Slides were then washed with Photoflo, and the film containing the nuclei was floated off the microscope slides onto the surface of distilled water. Grids were randomly placed on the film, and the film with grids was lifted from the water surface by Parafilm. Isolated grids were examined by transmission electron microscopy and electron micrographs acquired at magnifications between ×3,000 and ×15,000.

Fluorescence immunostaining of spread meiotic nuclei. Immunostaining of surface spreads of spermatocytes was performed as previously described[22]. Rabbit anti-SC(D), mouse anti-Cor1, mouse anti-Syn1, rabbit anti-histone H1t and human anti-centromere antibodies were used as previously described[22]. Rabbit anti-mouse Rad51 antibody was used as described[7]. Secondary antibodies conjugated with FITC or rhodamine were purchased commercially (Pierce).

Immunoblot analysis. Immunoblotting was performed directly on crude tissue samples by standard techniques[23]. A mixture of polyclonal antibodies to p53 (Ab-1 and Ab-3 from Oncogene and pAb 260 from Pharmingen), p21 (13436E from Pharmingen), Bax (06-449 from Upstate Biotechnology Institute) and relevant secondary antibodies (Amersham) were used for detection of these proteins. Total protein (50 μg) was loaded in each lane.

Acknowledgements

The authors would like to thank A. Shinohara and D. Chen for providing the Rad51 antibody; K. Brown for immunoblotting advice; D. Bishop for insight into meiosis; M. Dresser for helpful discussions about EM analysis of meiosis; D. Leja for assistance in figure preparation; M. Schröder, D. Larson and L. Garrett for excellent technical assistance; and R. Nussbaum for generous support. C.B. is a Clinical Endocrine Fellow supported by the National Institute of Diabetes, Digestive, and Kidney Diseases, and P.B.M. was financially supported by the National Research Council of Canada.

Received 18 July; accepted 14 October 1997.

1. Boder, E. Ataxia-telangiectasia: some historic, clinical and pathologic observations. *Birth Defects* **11**, 255–270 (1975).
2. Sedgewick, R. & Boder, E. Ataxia-telangiectasia. in *Handbook of Clinical Neurology* (eds Vinken, P., Bruyn, G. & Klawans, H.) 347–423 (Elsevier Scientific, New York, 1991).
3. Barlow, C. *et al.* Atm-deficient mice: a paradigm of ataxia telangiectasia. *Cell* **86**, 159–171 (1996).
4. Xu, Y. *et al.* Targeted disruption of ATM leads to growth retardation, chromosomal fragmentation during meiosis, immune defects, and thymic lymphoma. *Genes Dev.* **10**, 2411–2422 (1996).
5. Elson, A. *et al.* Pleiotropic defects in ataxia-telangiectasia protein-deficient mice. *Proc. Natl. Acad. Sci. USA* **93**, 13084–13089 (1996).
6. Lim, D.-S. & Hasty, P. A mutation in mouse *rad51* results in an early embryonic lethal that is suppressed by a mutation in *p53*. *Mol. Cell. Biol.* **16**, 7133–7143 (1996).
7. Moens, P.B. *et al.* Rad51 immunocytology in rat and mouse spermatocytes and oocytes. *Chromosoma* (in the press).
8. Baskaran, R. *et al.* Ataxia telangiectasia mutant protein activates c-Abl tyrosine kinase in response to ionizing radiation. *Nature* **387**, 516–519 (1997).
9. El-Deiry, W.S. *et al.* WAF1/CIP1 is induced in p53-mediated G1 arrest and apoptosis. *Cancer Res.* **54**, 1169–1174 (1994).
10. Miyashita, T. & Reed, J.C. Tumor suppressor p53 is a direct transcriptional activator of the human bax gene. *Cell* **80**, 293–299 (1995).
11. Jacks, T. *et al.* Tumor spectrum analysis in p53-mutant mice. *Curr. Biol.* **4**, 1–7 (1994).
12. Deng, C., Zhang, P., Harper, J.W., Elledge, S.J. & Leder, P. Mice lacking $p21^{CIP1/WAF1}$ undergo normal development, but are defective in G1 checkpoint control. *Cell* **82**, 675–684 (1995).
13. Moens, P.B. Histones H1 and H4 of surface-spread meiotic chromosomes. *Chromosoma* **104**, 169–74 (1995).
14. Scully, R. *et al.* Association of BRCA1 with Rad51 in mitotic and meiotic cells. *Cell* **88**, 265–275 (1997).
15. Sharan, S.K. *et al.* Embryonic lethality and radiation hypersensitivity mediated by Rad51 in mice lacking *Brca2*. *Nature* **386**, 804–810 (1997).
16. Hakem, R., de la Pompa, J.L., Elia, A., Potter, J. & Mak, T.W. Partial rescue of $Brca1^{5-6}$ early embryonic lethality by *p53* or *p21* null mutation. *Nature Genet.* **16**, 298–302 (1997).
17. Ludwig, T., Chapman, D.L., Papaioannou, V.E. & Efstratiadis, A. Targeted mutations of breast cancer susceptibility gene homologs in mice: lethal phenotypes of Brca1, Brca2, Brca1/Brca2, Brca1/p53, and Brca2/p53 nullizygous embryos. *Genes Dev.* **11**, 1226–1241 (1997).
18. Ko, L.J. & Prives, C. p53: puzzle and paradigm. *Genes Dev.* **10**, 1054–1072 (1996).
19. Levine, A.J. p53, the cellular gatekeeper for growth and division. *Cell* **88**, 323–331 (1997).
20. Luna, L.G. *Histopathological Methods and Color Atlas of Special Stains and Tissue* (American Histolabs, Gaithersburg, Maryland, 1992).
21. Dresser, M.E. & Moses, M.J. Silver staining of synaptonemal complexes in surface spreads for light and electron microscopy. *Exp. Cell Res.* **121**, 416–419 (1979).
22. Dobson, M.J., Pearlman, R.E., Karaiskakis, A., Spyropoulos, B. & Moens, P.B. Synaptonemal complex proteins: occurrence, epitope mapping and chromosome disjunction. *J. Cell Sci.* **107**, 2749–2760 (1994).
23. Harlow, E. & Lane, D. *Antibodies: A Laboratory Manual* (Cold Spring Harbor Laboratory, Cold Spring Harbor, New York, 1988).